PROGRESS REPORT ON THE FLAT BEAM EXPERIMENT AT THE FERMILAB/NICADD PHOTOINJECTOR LABORATORY

Y.-E Sun[*], K.-J. Kim, University of Chicago, Chicago, IL 60637, USA

P. Piot[†], K. Desler, H. Edwards, M. Hüning,

J. Santucci, J. Wennerberg, FNAL, Batavia, IL 60510, USA

N. Barov, Northern Illinois University, DeKalb, IL 60115, USA

R. Tikhoplav, University of Rochester, Rochester, NY 14627, USA

S. Lidia, LBNL, Berkeley, CA 94720, USA

Abstract

We report on our present progress toward the investigation on the generation of flat beam from an incoming angular momentum-dominated beam. In the present paper we compare our latest experimental results with numerical simulations.

INTRODUCTION

The generation of flat beam from an incoming angular momentum-dominated (magnetized) beam proposed in Reference [1] in the linear collider context has found, since then, other applications, e.g. in the linac-based light source [2]. A proof-of-principle experiment was performed at the Fermilab/NICADD photoinjector laboratory (FNPL) [3] and reported in various papers [4, 5]. In the present paper, we discuss the first results of a second series of experiment dedicated to better understand the production of magnetized beams and the subsequent removal of the longitudinal angular momentum with the round-to-flat beam (RTFB) transformer. The RTFB transformer (see
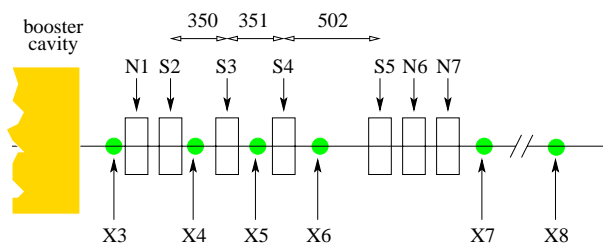

Figure 1: Overview of the RFTB section. The letters N, S and X represents normal and skew quadrupoles, and diagnostic stations. Dimension are in mm.

Fig. 1) consists of four skew quadrupoles located downstream of the booster cavity, at an energy $E \simeq 16$ MeV. Several optical transition radiation (OTR) or scintillating (YaG-based) screens allow the measurement of beam transverse density evolution through the RFTB transformer. The beam transverse emittances can be measured based on the multi-slit, or the quadrupole scan techniques. These emittance diagnostics are available both upstream and downstream of the RFTB section. Compared to the first series
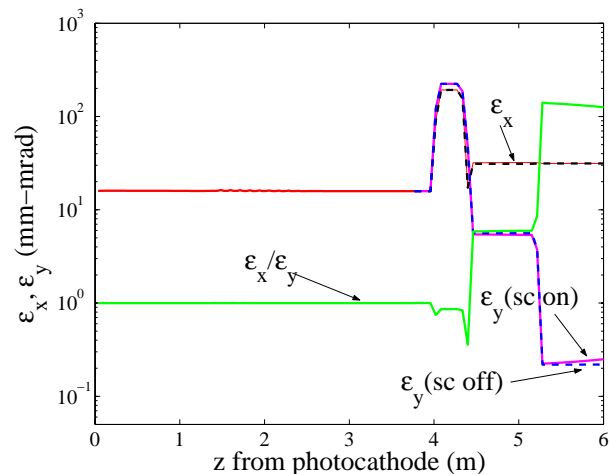

Figure 2: Simulated evolution of transverse emittances along the FNPL beamline for standard nominal settings.

Table 1: Typical settings for the rf-gun, accelerating section, and the photo-cathode drive-laser

parameter	value	units
laser injection phase	25 ± 5	rf-deg
laser radius on cathode	0.6-1.6 ($\pm$ 0.05)	mm
laser pulse duration	4 ($\pm$ 0.5)	ps
bunch charge	0.2-1.6	nC
E_z on cathode	34-35 $\pm$ 0.2	MV/m
B_z on cathode	200-1100	Gauss
booster cavity acc. gradient	~ 12	MV/m

of experiment, our main motivation for reorganizing the RFTB section was to locate all the RFTB section components upstream of the magnetic chicane. Such a relocation was motivated by the potential production of compressed flat beams at a later phase of the flat beam experiment. The typical operating parameters of the photo-injector sub-systems during data taking for the flat beam experiment are gathered in Table 1. A series of simulations were performed to study the performance of the RFTB section in term of what transverse emittance ratio could be achieved. An example of evolution of the transverse emittance along the beamline is presented in Fig. 2 for the a magneto-
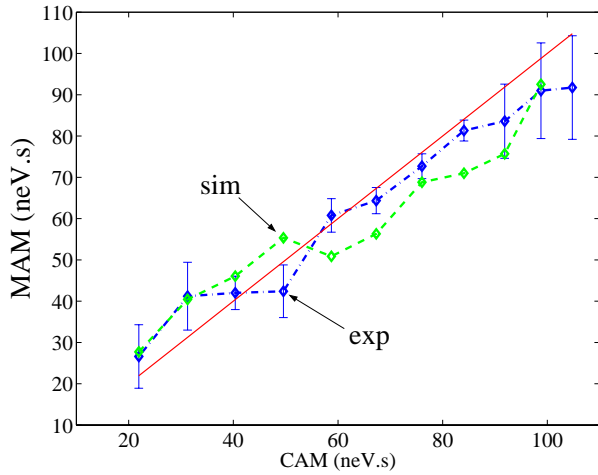
Figure 3: Mechanical angular momentum (MAM) compared to the canonical angular momentum (CAM) calculated from the longitudinal magnetostatic field at the photocathode. The labels "exp." and "sim." correspond respectively to experimentally measured data points and simulated value after modeling of the measurement technique.

static field $B_z = 829$ G on the photocathode surface (at $z = 0$ m). As one can see, this set of daily achievable beam parameters has the potential to generate a flat beam with transverse emittance ratio $\tilde{\varepsilon}_y/\tilde{\varepsilon}_x \simeq 31.39/0.23 \simeq 136$. We also note in Fig. 2 that space charge effects within the RFTB section are insignificant. But an increase of the smaller of the flat emittances is observed as the beam propagates downstream of the transformer − this is a critical issue that need to be taken into account when measuring the flat beam transverse emittances.

STUDY OF ANGULAR MOMENTUM-DOMINATED BEAMS

Given the B-field at the photocathode and the uncorrelated transverse emittance in the Larmor frame, ϵ_u, the flat beam transverse emittances, $\epsilon_\pm$, are respectively given by [6]:

$$\epsilon_\pm = \sqrt{\epsilon_u^2 + \mathcal{L}^2} \pm \mathcal{L}, \text{ with } \mathcal{L} = \kappa\sigma_c^2, \quad (1)$$

wherein σ_c is the rms drive-laser spot size on the photocathode and $\kappa \doteq eB_z/(2p)$, e is the electron charge, B_z the longitudinal magnetic field on photocathode and p the particle momentum. For a cylindrically symmetric beam, $\mathcal{L}$ is related to the canonical angular momentum through [7]:

$$\langle L \rangle = 2p\mathcal{L}. \quad (2)$$

We use the technique to measure the mechanical angular momentum from a measurement of beam rms spot sizes, σ_1 and σ_2, at two longitudinal locations z_1 and $z_2(> z_1)$ and the measurement of rotation angle, θ, of beamlets pattern at z_2 produced by inserting a multi-slit mask at loca-

tion z_1: the averaged mechanical angular momentum is obtained from $\langle L \rangle = p\sigma_1\sigma_2 \sin\theta/(z_2 - z_1)$.

A set of measurement of the evolution of mechanical angular momentum evolution versus B-field on the photocathode was reported in Ref. [7]. Here such an experiment was performed varying the B_z-field over a wider range ($B_z \in [200, 1100]$ Gauss) − see details in Ref. [8]. The measurement technique aforementioned was also numerically tested for each experimental data point. In Figure 3 we compare the measured mechanical angular momentum with the canonical angular momentum calculated, given the B-field on the photocathode, from Eq.2. The measured val-
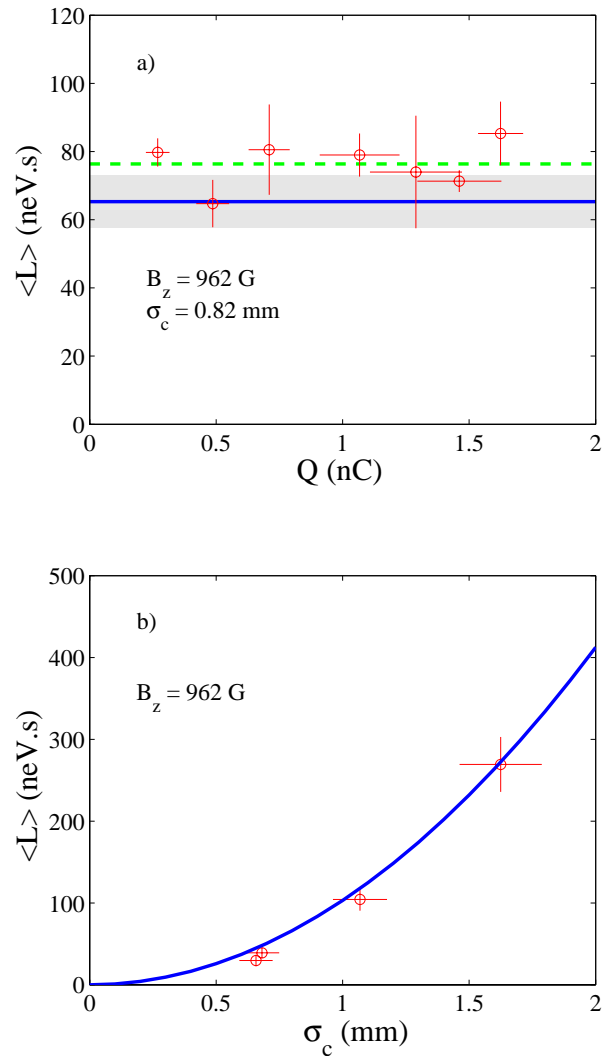

Figure 4: Angular momentum versus charge **a)** and photocathode drive-laser spot size **b)**. The experimental data (circles) are compared with theoretical value of the canonical angular momentum calculated from the longitudinal magnetostatic field. In **a)**, the dashed line represent the average value of all the data points, and the shaded area corresponds to the uncertainty on the canonical angular momentum.

ues include both experimental data and simulated values, i.e. values that have been retrieved after a numerical simulation of the measurement.

The dependence of angular momentum on the charge was also explored, in this experiment the laser spot size was set to $\sigma_c = 0.98$ mm, and laser intensity was varied by the mean of a wave plate attenuator located in the ultraviolet path of the laser. The results, shown in Fig. 4(a), indicate the angular momentum is charge-independent, confirming our assumption that the beam dynamics is angular momentum-dominated.

Finally the dependence of angular momentum versus σ_c was investigated, in this experiment σ_c was varied using a remotely controllable iris. The laser intensity was held constant and the B-field on the photocathode was identical to the previous experiment ($B_z = 962$ G). The measurements (see Fig. 4(b)) support the expected quadratic dependence of the angular momentum on σ_c.

REMOVAL OF ANGULAR MOMENTUM

The incoming angular momentum-dominated beam is converted into a flat beam using only three quadrupoles (S2, S3, S5 in Fig. 1) for the series of measurement presented hereafter. Given the photoinjector parameters, numerical simulations of the upstream beamline are performed using the tracking program ASTRA[9]. From the transverse phase space obtained at the transformer entrance, the correlation matrix defined as $\mathcal{C} \doteq \langle Y\widetilde{X}\rangle\langle X\widetilde{X}\rangle^{-1}$ is calculated, wherein $\widetilde{X} = (x, x')$, $\widetilde{Y} = (y, y')$ and $\sim$ stands for the transpose operator. The required skew quadrupole strengths are then computed such that the quantity $\chi^2 \doteq \sum_i \sum_j |\mathcal{C}_{i,j}|^2$ evaluated downstream of the RFTB transformer is minimized. The starting values for the minimization algorithm are the one derived under the thin lens approximation in Reference [5].

Experimentally further optimization around the predicted values is generally needed to insure the angular momentum is totally suppressed (as inferred by observation of the x-y coupling at several location downstream of the RFTB section). Presently we observed an agreement between the predicted values and those experimentally optimized of about 10 to 20%. The evolution of beam transverse density throughout the RFTB section is in very good agreement with the expectations from simulation, as depicted in Figure 5.

SUMMARY AND FUTURE PLANS

The dependence of mechanical angular momentum on B-field, charge and laser spot size on the cathode have been measured. A new configuration for the round-to-flat beam transformer has been commissioned, and good qualitative agreement is observed between numerical simulations and experiment. To date we have not yet attempted to precisely measure the achieved emittance: further work on the emittance measurement is first needed.
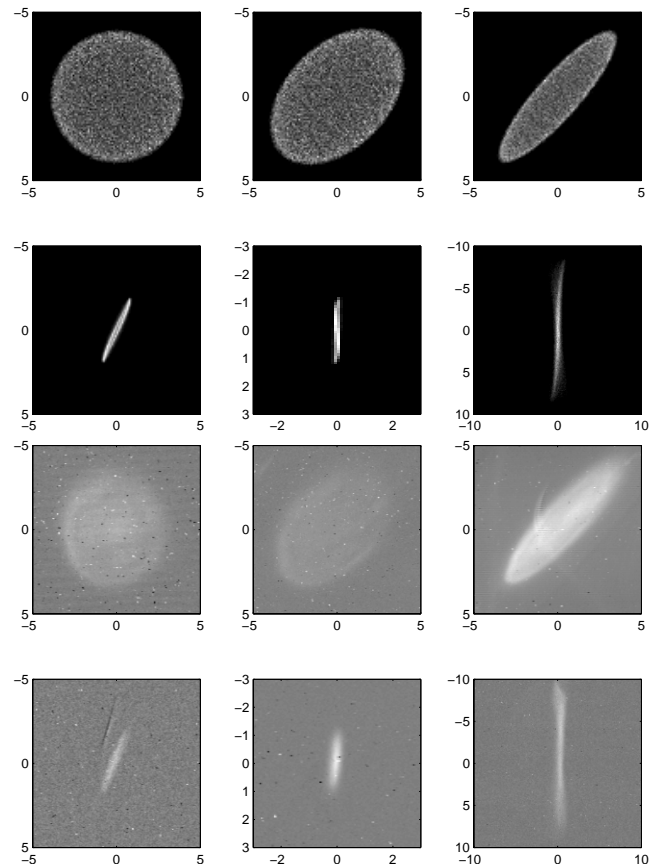

Figure 5: Simulated (top six plots) and measured (bottom six plots) beam transverse density evolution in the RFTB section. The consecutive plots corresponds to location X3, X4, X5, X6, X7 and X8. Dimensions are in mm.

ACKNOWLEDGEMENTS

REFERENCES

[1] R. Brinkman *et al.*, *Phys. Rev. ST A&B* **4**, 053501 (2001)

[2] J. Corlett *et. al*, proc. EPAC 2002, 668-670 (2002)

[3] K. Desler et. al, this conference

[4] D. Edwards *et al.*, proc. LINAC 2000, 122-124 (2000)

[5] E. Thrane *et al.*, proc. LINAC 2002, 308-310 (2002)

[6] K.-J. Kim *et al.*, *Phys. Rev. ST A&B* **6**, 104002 (2003)

[7] Y.-E Sun *et al.*, proc. PAC 2003, 2682-2684 (2003)

[8] Y.-E Sun and P. Piot, Beams Document 1254-v1 July 2004 (unpublished) available at http://beamdocs.fnal.gov/cgi-bin/public/DocDB/DocumentDatabase

[9] K. Flöttman, *Astra user manual* DESY